Hydrol. Earth Syst. Sci., 21, 1117–1135, 2017
www.hydrol-earth-syst-sci.net/21/1117/2017/
doi:10.5194/hess-21-1117-2017

Hydrology and Earth System Sciences
Open Access
EGU

Systematic shifts in Budyko relationships caused by groundwater storage changes

Laura E. Condon[1] **and Reed M. Maxwell**[2]

[1]Department of Civil and Environmental Engineering, Syracuse University, Syracuse, NY, USA
[2]Integrated GroundWater Modeling Center, Department of Geology and Geological Engineering, Colorado School of Mines, Golden, CO, USA

Correspondence to: Laura E. Condon (lecondon@syr.edu)

Received: 13 August 2016 – Discussion started: 24 August 2016
Revised: 3 February 2017 – Accepted: 6 February 2017 – Published: 22 February 2017

Abstract. Traditional Budyko analysis is predicated on the assumption that the watershed of interest is in dynamic equilibrium over the period of study, and thus surface water partitioning will not be influenced by changes in storage. However, previous work has demonstrated that groundwater–surface water interactions will shift Budyko relationships. While modified Budyko approaches have been proposed to account for storage changes, given the limited ability to quantify groundwater fluxes and storage across spatial scales, additional research is needed to understand the implications of these approximations. This study evaluates the impact of storage changes on Budyko relationships given three common approaches to estimating evapotranspiration fractions: (1) determining evapotranspiration from observations, (2) calculating evapotranspiration from precipitation and surface water outflow, and (3) adjusting precipitation to account for storage changes. We show conceptually that groundwater storage changes will shift the Budyko relationship differently depending on the way evapotranspiration is estimated. A 1-year transient simulation is used to mimic all three approaches within a numerical framework in which groundwater–surface water exchanges are prevalent and can be fully quantified. The model domain spans the majority of the continental US and encompasses 25 000 nested watersheds ranging in size from 100 km^2 to over 3 000 000 km^2. Model results illustrate that storage changes can generate different spatial patterns in Budyko relationships depending on the approach used. This shows the potential for systematic bias when comparing studies that use different approaches to estimating evapotranspiration. Comparisons between watersheds are also relevant for studies that seek to characterize variability in the Budyko space using other watershed characteristics. Our results demonstrate that within large complex domains the correlation between storage changes and other relevant watershed properties, such as aridity, makes it difficult to easily isolate storage changes as an independent predictor of behavior. However, we suggest that, using the conceptual models presented here, comparative studies could still easily evaluate a range of spatially heterogeneous storage changes by perturbing individual points to better incorporate uncertain storage changes into analysis.

1 Introduction

The Budyko hypothesis states that the fraction of precipitation (P) that leaves a watershed through evapotranspiration (E), as opposed to runoff, can be predicted by the aridity of the watershed (Budyko, 1958, 1974). Budyko (1974) compared long-term evapotranspiration fractions to aridity for 1200 large watersheds around the globe and showed that 90 % of the variance in evapotranspiration ratio (E / P) could be described by a single empirical curvilinear equation dependent only on aridity, often referred to as the "Budyko Curve". Budyko noted that this consistent relationship is a reflection of the dominance of macroclimate over large drainage areas and long time periods where it can be assumed that a watershed is in steady state (i.e., when it can be assumed that there are no storage changes over the period of analysis).

The simplicity of this relationship has since garnered much interest within the hydrologic community for its potential to predict watershed behavior using only climate variables, which are often easier to observe than many hydrologic variables, and without relying on computationally expensive or heavily parameterized numerical models. In recent years, the Budyko hypothesis has also been put forward as a way of predicting hydrologic sensitivity to climate change, especially in ungauged basins (e.g., Donohue et al., 2011; Jones et al., 2012; Renner et al., 2014). However, application of this method has been partially limited by spatial variability between watersheds and the required steady-state assumption.

The original Budyko curve presented a universal relationship between evapotranspiration and aridity (Budyko, 1974). Subsequent work has shown that, while the Budyko curve is generally robust, climate alone is not sufficient to predict watershed partitioning; the shape of the curve can vary between locations, especially for smaller watersheds. Differences in behavior between river basins have been attributed to seasonal lags in water and energy supply and vegetative and soil properties (Donohue et al., 2007). The original Budyko curve has been reformulated multiple times to incorporate additional free parameters to reflect these differences (Choudhury, 1999; Fu, 1981; Milly, 1994; Zhang et al., 2001, 2004), and numerous studies have used these modified formulations to relate curve parameters to physical basin characteristics in many settings (e.g., Li et al., 2013; Shao et al., 2012; Williams et al., 2012; Xu et al., 2013; Yang et al., 2009). For example, Li et al. (2013) and Yang et al. (2009) evaluated relationships between the shape of the Budyko curve and vegetation coverage. Similarly, Williams et al. (2012) and Zhang et al. (2004) found distinct shape parameters when comparing forested watersheds to grasslands, although it should be noted that they reached the opposite conclusion about their relative magnitudes. Others have focused on the role of soil moisture and noted differences in behavior based on plant water availability and seasonal lags in supply and demand (e.g., Milly, 1994; Yang et al., 2007; Yokoo et al., 2008).

Many previous studies have demonstrated good predictive abilities using modified Budyko formulations even when applied to smaller watersheds and shorter timescales than those originally intended. However, poor performance in some locations, especially over annual or seasonal time periods, has been attributed to the influence of storage changes that violate the steady-state assumption (Milly and Dunne, 2002; Zhang et al., 2008). Istanbulluoglu et al. (2012) and Wang et al. (2009) showed interannual storage changes can produce a negative correlation between the evapotranspiration ratio and aridity that is counter to the Budyko curve for baseflow-dominated basins in the Nebraska Sand Hills. Wang (2012) evaluated inter-annual storage changes for twelve watersheds in Illinois and showed that, on an annual timescale, variability in runoff and storage is larger than evapotranspiration, and accounting for storage can improve the performance of Budyko predictions. Du et al. (2016) presented a method for explicitly accounting for storage changes within the Budyko framework and demonstrated that this approach can greatly improve performance in arid regions, or over shorter timescales where the steady-state assumption is not valid.

These studies all indicate the potential importance of groundwater–surface water interactions within the Budyko framework and illustrate paths forward for incorporating groundwater–surface water interactions into Budyko analysis. However, the extensive field work needed to fully quantify groundwater–surface water exchanges is often not possible and is counter to the simplicity and minimal data requirements of the Budyko approach. Even in Budyko analysis focused on groundwater–surface water interactions, quantifying groundwater changes remains a limiting factor. For example, in some studies, the impact of groundwater storage changes have been inferred from variability around the Budyko relationship without directly measuring these changes (Milly and Dunne, 2002; Zhang et al., 2008). Others have addressed interactions more directly using baseflow separation techniques that require only streamflow observations (Wang et al., 2009) or lumped watershed models that parameterize baseflow and recharge (Du et al., 2016). However, with both of these approaches the groundwater system is still not directly simulated or observed. Istanbulluoglu et al. (2012) and Wang (2012) did use observations of water table depth to directly quantify storage changes and demonstrate the impact of this change within the Budyko framework; but the study areas with this approach were relatively limited (four watersheds for Istanbulluoglu et al., 2012, and twelve for Wang, 2012). Groundwater observations sufficient to precisely characterize watershed storage changes are difficult to obtain and are not widely available. Therefore, adding groundwater storage calculations into Budyko analyses remains infeasible in many cases, and more work is needed to understand the sensitivity of Budyko relationships to changes in storage.

There are three common approaches to estimating evapotranspiration (E) in Budyko analysis (listed here in order of complexity): first, if E cannot be measured directly, it is often estimated as the difference between precipitation and river outflow in a basin. Second, E can be measured directly using a variety of field methods. Third, as is the case with the more recent studies that seek to account for storage changes, observed E values can be augmented with measurements of groundwater–surface water exchanges to estimate the "effective precipitation" that is available for surface processes (i.e., outflow and E). Here we hypothesize that storage changes will bias Budyko results in predictable ways, as has been indicated by previous studies, but that the direction of the bias will vary based on the way that evapotranspiration is handled within a study. We evaluate this hypothesis by comparing Budyko relationships generated following the three different approaches using the outputs of a physically based hydrologic model that directly simulates the integrated

groundwater–surface water system over a large spatial domain at high resolution. The three primary goals of our comparative analysis are as follows:

1. evaluate the sensitivity of Budyko relationships to groundwater storage changes;
2. characterize systematic differences in the impact of storage changes on Budyko relationships;
3. illustrate variability between approaches across physical settings and spatial scales.

2 Methods

We use an integrated hydrologic model to simulate water and energy fluxes in both the surface and the subsurface. Here we apply a high-resolution (1 km^2) simulation of the majority of the continental US which covers more than 6 million km^2 and simulates hydrologic systems across a broad range of physical settings and storage change magnitudes. The model is driven using historical observed atmospheric forcings such as precipitation and temperature, and provides gridded outputs of all water and energy fluxes throughout the system. We use simulated surface water flow, evapotranspiration and groundwater–surface water exchanges to calculate Budyko relationships, using three different approaches to estimating fluxes:

1. calculating evapotranspiration from simulated runoff and precipitation;
2. using simulated evapotranspiration values directly;
3. using simulated evapotranspiration values directly and taking into account storage changes.

Differences between the approaches are compared with storage changes in each basin to evaluate the systematic impacts of these changes on Budyko relationships.

The numerical modeling approach used here provides several important advantages for this type of analysis. Within the model, groundwater–surface water exchanges for every watershed in the system are fully characterized. This guarantees perfect closure of the water balance and means that we can mimic all three approaches within a consistent numerical framework where storage changes are directly accounted for. Furthermore, because the goal is to understand differences between approaches, and not to predict local Budyko parameters, the key advantage here is the ability to evaluate physically realistic behavior across a variety of physical settings and spatial scales where groundwater can be fully accounted for. Within this context, it should also be noted that the focus is on how groundwater storage changes perturb relationships. Therefore, uncertainty in local model parameters is much less important than realistic simulation of physical interactions for a range of storage changes and aridity values within a controlled numerical framework.

Sections 2.1 and 2.2 detail the numerical modeling approach and the continental-scale simulation used for analysis. An explanation of the source of each of the relevant water balance terms generated from the model is provided in Sect. 2.3. Sections 2.4 and 2.5 explain the three different approaches for ET estimation and how they are evaluated within the Budyko Framework.

2.1 Hydrologic modeling

Previous work has evaluated the Budyko curve using hydrologic models of varying levels of complexity. The "abcd" model employed by Du et al. (2016), among others, is a lumped water balance model that includes baseflow and groundwater recharge using calibrated parameters. Yokoo et al. (2008) used a different water balance model with a more complex groundwater formulation that includes saturated and unsaturated zones, but the authors noted limitations in simulating infiltration excess overland flow with this approach. Gentine et al. (2012) applied a water balance model that includes a soil bucket and can simulate infiltration excess overland flow; however it did not include topography and was only applied at the plot scale. While these approaches do account for storage in the subsurface, and varying levels of complexity in groundwater–surface water exchanges, they all take a lumped approach and rely on calibrated parameters that are not physically based. The lumped parameter approach is illustrated in Fig. 1a.

Increasing in sophistication, Troch et al. (2013) used a semi-distributed model that included shallow perched aquifers as well as root zone and soil moisture dynamics; and Koster and Suarez (1999) evaluated a global circulation model that simulated land surface and atmospheric processes using physically based equations. Incorporating more sophisticated physical processes increases computational expense, especially for large high-resolution domains. To address this, Koster and Suarez (1999) used a global simulation but at low spatial resolution (4° by 5°), while Troch et al. (2013) limited their analysis to the hillslope scale. Furthermore, both of these approaches are focused on the land surface and shallow subsurface and neither included lateral groundwater flow as shown in Fig. 1b.

To the authors' knowledge, no one has evaluated Budyko behavior over large spatial scales using a hydrologic model that integrates lateral groundwater flow with surface processes (Fig. 1c). So-called integrated hydrologic models that incorporate physically based lateral groundwater flow with overland flow and land surface processes are a relatively new development in hydrologic modeling. These tools are ideal for capturing dynamic behavior and interactions throughout the terrestrial hydrologic cycle and they have been increasingly applied over the last decade. Achieving this level of complexity requires significant computational resources and

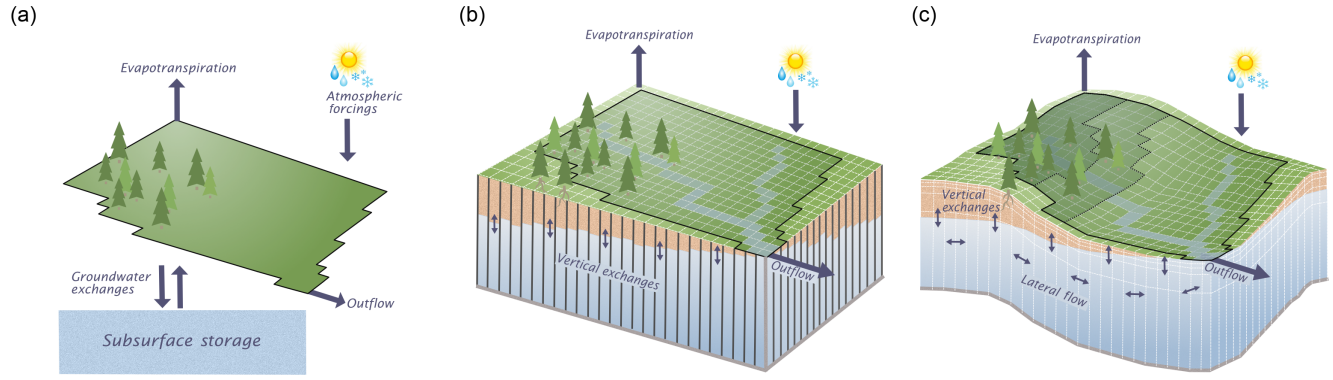

Figure 1. Conceptual illustration of **(a)** lumped parameter hydrologic models, **(b)** land surface models with vertical subsurface exchanges and **(c)** integrated hydrologic models. The nested subbasin approach is also illustrated on **(c)** using the black outlines for reference.

detailed model inputs. These requirements have generally limited the application of integrated tools to regional-scale domains. Continental-scale high-resolution simulations have only recently become technically feasible.

For this analysis, we use the first high-resolution integrated groundwater–surface water simulation of the majority of the continental US (CONUS) (Maxwell and Condon, 2016; Maxwell et al., 2015). The CONUS simulation was developed using the integrated hydrologic model ParFlow–CLM (Kollet and Maxwell, 2006, 2008; Maxwell and Miller, 2005). ParFlow simulates three-dimensional variably saturated groundwater flow using Richards' equation:

$$S_s S\left(\psi_p\right)\frac{\delta\psi_p}{\delta t}+\phi\frac{\delta S\left(\psi_p\right)}{\delta t}=\nabla\cdot\left[-K_s(x)k_r\left(\psi_p\right)\cdot\nabla\left(\psi_p-z\right)\right]+q_s, \quad (1)$$

where S_s is the specific storage (L^{-1}), S is the relative permeability (–) (which varies with pressure head ψ_p (L) based on the Van Genuchten (1980) relationships), t is time (T), φ is the porosity of the subsurface (–), $K_s(x)$ is the saturated hydraulic conductivity tensor ($L\,T^{-1}$), K_r is the relative permeability (–) (which also varies with pressure head according to the Van Genuchten (1980) relationships), z is the depth below the surface (L) and q_s is a source–sink term (T^{-1}). Note that units of T^{-1} for the flux terms reflect the fact that they are scaled by the cell thickness.

Overland flow is included in the groundwater flux term of Eq. (1) (i.e., in the first term on the right hand side) using a free surface overland-flow boundary condition that applies continuity of pressure and flux across the boundary between the land surface and the subsurface. Overland flow is solved using the kinematic wave approximation of the momentum equation where the diffusion terms are neglected and it is assumed that the bed slope, S_0 (–), is equivalent to the friction slope. Flow varies as a function of ponded depth according to Manning's equation:

$$v=\frac{\sqrt{S_0}}{n}\psi_p^{2/3}, \quad (2)$$

where n ($T\,L^{-1/3}$) is the Manning roughness coefficient. Using this approach ParFlow is able to solve variably saturated groundwater flow and overland flow simultaneously. Practically this means that (1) the location of surface water bodies do not need to be specified a priori and will develop wherever water ponds in the domain, and (2) two-way groundwater–surface water exchanges can evolve dynamically based on head gradients and subsurface properties.

ParFlow is also coupled with a land surface model derived from the Common Land Model (CLM) (Dai et al., 2003). In the combined ParFlow–CLM model (Kollet and Maxwell, 2008), ParFlow solves the water balance in the subsurface and CLM solves the combined water energy balance at the land surface. At the land surface, the energy balance (R_{net}) is comprised of sensible (H), latent (LE) and Ground (G) heat fluxes ($W\,m^{-2}$):

$$R_{net}=H+LE+G. \quad (3)$$

All of the energy fluxes listed in Eq. (3) vary with soil moisture. CLM uses pressure head and saturation values for the upper subsurface layers (in this case the top 2 m) simulated by ParFlow and passes infiltration fluxes back to ParFlow. Land surface processes are also driven by atmospheric forcing variables, which are provided as inputs to the model. Forcing variables include short- and long-wave radiation, precipitation, air temperature, atmospheric pressure, specific humidity and wind. Using these inputs, CLM simulates multiple land surface processes including canopy interception, evaporation from the canopy and the ground surface, plant transpiration, ground and sensible heat fluxes as well as snow dynamics.

This study focuses on simulated evapotranspiration E ($L\,T^{-1}$), which is the sum of evaporation Ev, and plant transpiration T. CLM uses a mass-transfer approach with mean

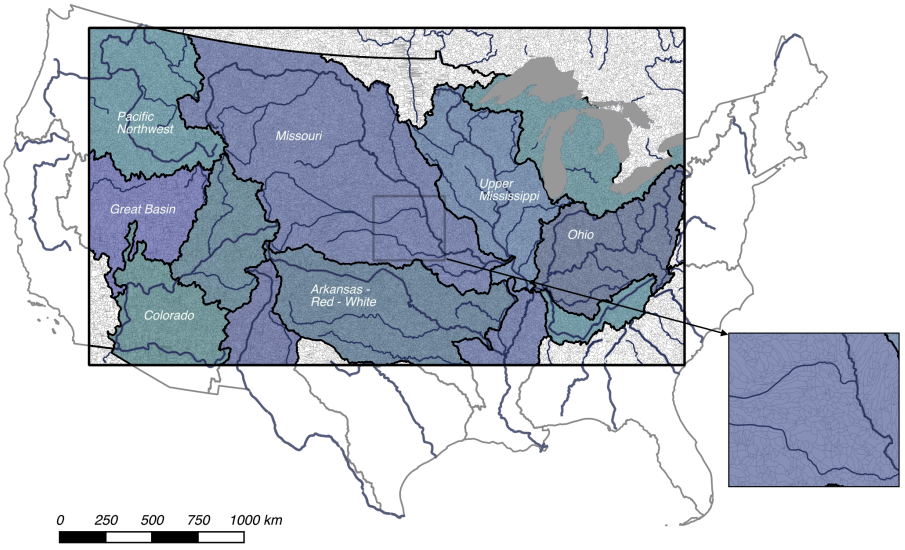

Figure 2. Map of the simulation domain extent (black box) with major river basins highlighted and labeled. Subbasins within the domain are outlined in grey. Major rivers are shown in blue for reference (note that the simulated river network is much more highly resolved, as illustrated in Maxwell et al., 2015).

variables where evaporation is calculated using the gradient between the specific humidity at the ground surface, q_g (mm^{-1}), and the specific humidity at a reference height, q_a (mm^{-1}), scaled by a soil resistance factor β (–), air density ρ_a and the atmospheric resistance, r_d (–) as follows:

$$Ev = -\beta \rho_a \frac{q_g - q_a}{r_d}. \quad (4)$$

The soil resistance factor is calculated based on the saturation relative to the residual saturation and the saturation in the uppermost soil column (refer to Jefferson and Maxwell, 2015, for the complete formulation).

Similarly, transpiration is calculated by scaling the potential evapotranspiration to account for stomatal and aerodynamic resistance as follows:

$$T = \left(R_{pp,dry} + L_w\right) L_{SAI} \left(\rho_a \frac{q_{sat} - q_a}{r_d}\right). \quad (5)$$

Here $R_{pp,dry}$ (–) is a scaling parameter, L_w (–) is the fraction of the canopy that is covered in water, L_{SAI} is leaf and stem area index and q_{sat} (–) is the saturated specific humidity (mm^{-1}). $R_{pp,dry}$ is a function of light and moisture limitations. Parameters that are used to determine leaf area index, reflectance and transmittance and root distributions vary by land-cover type and are provided as inputs to the model using the 18 land-cover classes defined by the International Geosphere–Biosphere Programme (IGBP). For additional details on the numerical approach and analysis on the sensitivity of evaporation and transpiration within the CLM the reader is referred to Ferguson et al. (2016) Jefferson and Maxwell (2015), Kollet and Maxwell (2008) and Maxwell and Condon (2016).

2.2 Model domain and simulations

The analysis presented here is based on a previously developed transient ParFlow–CLM simulation of the majority of the CONUS documented in Maxwell and Condon (2016). The CONUS domain covers the majority of eight major river basins, shown in Fig. 2, and spans roughly 6.3 million km^2 at 1 km lateral resolution. The integrated physically based approach employed for this simulation requires significant computational resources. However, there are several key benefits that warrant this costly approach; this simulation (1) provides high-resolution (1 km^2) gridded outputs that fully define water and energy fluxes from the groundwater through the land surface without calibration, (2) requires a minimal number of empirical parameters and (3) directly simulates variably saturated lateral groundwater flow which has not been incorporated in previous models used for Budyko analysis.

As detailed in Maxwell and Condon (2016) and Maxwell et al. (2015), the model extends 102 m below the subsurface, with five vertical layers that contour to the land surface using a terrain following grid formulation (Maxwell, 2013). The vertical resolution of the domain decreases with depth to better resolve the shallow subsurface. Layer thicknesses are 0.1, 0.3, 0.6, 1 and 100 m moving from the land surface down. Spatially heterogeneous physical parameters for the subsurface include porosity, saturated hydraulic conductivity and van Genuchten parameters. Subsurface spatial units were determined using a national permeability map developed by Gleeson et al. (2011) for the bottom 100 m of the domain and the soil survey geographic database (SSURGO) for the top 2 m. Maps of the subsurface units and their properties

are available in Maxwell and Condon (2016) and Maxwell et al. (2015). The land surface was derived from the hydrologic data and maps based on the shuttle elevation derivatives at multiple scales (HydroSHEDS) digital elevation model using a topographic processing algorithm to ensure a fully connected drainage network (Barnes et al., 2016). Vegetation types were extracted from the USGS land-cover dataset using the IGBP land-cover classifications.

The model was first initialized to a steady-state groundwater configuration, using the ParFlow model without CLM, starting from a completely dry domain and providing a constant recharge forcing over the land surface to achieve a dynamic equilibrium. Development of this steady-state simulation and evaluation of the resulting groundwater configuration are provided in Condon et al. (2015) and Maxwell et al. (2015). Using the steady-state groundwater configuration as a starting point, and following some initialization period, the coupled ParFlow–CLM model was used to simulate the fully transient system including land surface processes for water year 1985 (i.e., 1 October 1984 through 30 September 1985), which was chosen as it is the most climatologically average within the past 30 years. The transient simulation was driven by historical hourly meteorological forcings for water year 1985 from the North American Land Data Assimilation System Phase 2 (NLDAS 2) (Cosgrove et al., 2003; Mitchell et al., 2004). Anthropogenic activities such as groundwater pumping and surface water storage are not included in the transient simulation. Therefore the simulation represents natural flows in a pre-development scenario, which is ideal for Budyko analysis. Complete details of the development of the transient simulation are available in Maxwell and Condon (2016).

The 1-year simulation presented here intentionally violates the steady-state assumption. The purpose of our analysis is to evaluate the impact of net storage changes on Budyko relationships, and therefore a steady-state simulation is not the goal. It can also be argued that storage changes will vary from year to year or depending on the multi-year period analyzed. The 1985 simulation year is not presented as a prediction of long-term storage variability, it is simply used to sample a range of groundwater–surface water exchanges across variable climates and physical settings. We present a general framework for understanding the impacts of storage changes in various Budyko formulations using water year 1985 as a representative example.

Similarly, because we are focused on a comparative analysis within the Budyko framework, the results are not dependent on local calibration between simulated results and observations. The discrepancies between approaches stem from differences in the variables used to create a water balance (refer to Sects. 2.3 and 2.4); these findings are not sensitive to parameter uncertainty in the model. Still, the transient simulation has been rigorously validated against all publicly available observations for water year 1985. This includes transient observations at varying frequencies from 3050 stream gauges, 29 385 groundwater wells and 378 snow stations for a total of roughly 1.2 million comparison points. Flux tower observations were not available over this period, but latent heat fluxes were also compared to the Modern Era Retrospective-analysis for Research and Application (MERRA) dataset. Complete details of the model validation are provided in the Supplement of Maxwell and Condon (2016).

Although there are of course limitations to the model and significant uncertainties in spatial model parameterization, especially for the subsurface, overall comparisons between simulated and observed values demonstrate that the modeling approach is robust. Stream-flow timing and magnitude are generally well matched in undeveloped basins, snowpack timing and melt is accurate, and spatial patterns in latent heat flux are reasonable. Most importantly for this analysis, the model validation shows that ParFlow is accurately capturing the relevant physical processes. Uncertainty in subsurface parameterization, bias in atmospheric forcing data and lack of anthropogenic activities were identified as key areas that could improve the local predictions of the model. However, as discussed above, the purpose of this work is not to predict Budyko curve parameters for water year 1985. The uncertainties listed here are therefore important to note, but do not limit the utility of this tool as a test bed for evaluating interactions across spatial scales and complex physical settings.

2.3 Water balance components

Outputs from the hydrologic simulation are used to quantify all of the relevant water balance components for Budyko analysis. Precipitation is an input to the ParFlow CLM model. Within the model, precipitation can infiltrate to the subsurface, contribute to runoff or pond on the land surface. Evaporation occurs from ponded water, bare soil and canopy interception. Additionally, roots pull water from the subsurface to support transpiration for plants and lateral groundwater flow redistributes moisture within the subsurface and can further support overland flow. All of these processes occur within every 1 km^2 grid cell in the domain. The focus of this work is on watershed function and therefore the gridded results are aggregated to more hydrologically relevant units. The domain is divided into 33 454 subbasins, each containing a single stream. Subbasin areas, outlined in Fig. 2, vary but are generally on the order of 100 km^2. The total drainage area for every subbasin, henceforth referred to as the watershed, is defined by tracing up the river network to encompass the entire upstream contributing area. This results in 33 454 nested watersheds ranging in drainage area from about 100 to over 3 million km^2. For all of the following analysis we will focus on the 24 235 watersheds that are contained within the highlighted regions of Fig. 2. Similarly, while the simulation uses an hourly time step, here we evaluate annual values.

At the watershed scale, precipitation P (L^3) is balanced by surface water outflows, Q_{out} (L^3), evapotranspiration, E (L^3), and net groundwater–surface water exchanges, referred to as groundwater contributions, G (L^3).

$$P = Q_{out} + E + G \tag{6}$$

Equivalently this can be expressed in terms of ratios relative to incoming precipitation where the sum of the outflow ratios sum to 1:

$$1 = \frac{Q_{out}}{P} + \frac{E}{P} + \frac{G}{P}. \tag{7}$$

As noted above, every watershed fully encompasses its contributing area, and therefore surface water inflows are zero. P is the sum of the gridded annual precipitation over the drainage area. Every watershed is defined as having a single outlet point. Q_{out} is the overland flow calculated hourly at the outlet using the ponded water depth from Eq. (2) and summed over the simulation period. E is the total evaporation and transpiration simulated by ParFlow–CLM summed for every grid cell in the drainage area over the year.

There are multiple ways to estimate groundwater contributions within the model. Using gridded model outputs, the exchanges across the boundaries of every river cell can be summed to determine net contribution of groundwater to overland flow. Similarly, we can aggregate hourly changes in groundwater storage for every subbasin to determine total storage exchanges. Because we are interested in the net contribution of groundwater to streamflow and evapotranspiration for this analysis, we can take a simpler approach here. Within our numerical framework we have guaranteed closure of the water balance for every watershed and therefore the net change in groundwater storage that contributes to the surface water budget is simply $P - Q_{out} - E$, based on Eq. (6). When calculated this way, G encompasses the total groundwater–surface water exchanges (i.e., changes in storage) required to support the simulated outflow and evapotranspiration. It should be noted that in this formulation G encompasses both exchanges between groundwater and surface water, which can be either positive fluxes from the surface to the subsurface or negative fluxes from subsurface to the surface, as well as changes in surface water storage. The assumption is that, over the annual simulation, changes in ponded water are small relative to groundwater–surface water exchanges and so we simply refer to G as groundwater storage changes or groundwater contributions. We follow the convention that a positive groundwater contribution denotes water that is infiltrating from the land surface to the subsurface whereas a negative value indicates groundwater discharge which can either occur from groundwater-supported E or baseflow contributions to streams.

This approach is focused solely on the net contribution of groundwater to the surface water budget. Nested systems of local and regional lateral groundwater flow are simulated within the model and previous work has evaluated spatial patterns and physical drivers of lateral groundwater imports and exports across the domain (Condon et al., 2015; Maxwell et al., 2015) as well as groundwater residence times (Maxwell et al., 2016). Here we focus only on net exchanges with the surface that are relevant to the Budyko formulation. We do not need to quantify lateral exchanges in the subsurface directly for these purposes; however, it should be noted that the lateral redistribution of groundwater that occurs within the model is still vital to generating realistic groundwater configurations and supporting groundwater–surface water exchanges.

In addition to the simulated evapotranspiration (E), potential evaporation E_p is calculated using Eq. (4), the hourly meteorological forcing data used to drive the simulations (air temperature, atmospheric pressure, specific humidity and wind speed), and simulated ground temperatures in the uppermost layer of the model. To calculate potential evaporation, as opposed to E, the β parameter is set to 1 to eliminate soil resistance and q_g is the saturated specific humidity calculated based on the ground temperature and atmospheric pressure. This approach is designed to be consistent with the CLM simulation of ET but is slightly simplified because it does not evaluate atmospheric stability (refer to Jefferson and Maxwell, 2015, for a detailed comparison of different formulations). As with E, hourly gridded E_p values are summed over the entire simulation period for every watershed drainage area. Using the modeled simulated ground temperatures and model inputs to calculate E_p ensures that the E_p values driven by the same water and energy inputs that control E in the simulation.

Figure 3 maps the aridity index (E_p/P) as well as each component of the water balance from Eq. (7) expressed as ratios of precipitation. Figure 3b and c show regional trends in the relative importance of evapotranspiration as opposed to overland flow. In the more arid western portions of the domain (shown in red in Fig. 3a), Q_{out} is small compared to E, whereas in the more humid eastern portions of the domain (blue and orange values in Fig. 3a) the relative magnitude of Q_{out} increases.

Within this annual simulation, Fig. 3d shows that groundwater–surface water exchanges (G/P) can be a substantial portion of the water balance in much of the domain. This indicates that the system in not in steady state over the simulation period. As discussed in Sect. 2.2, the 1-year simulation time was intentionally selected for this reason. Here, we take advantage of the ability to directly calculate groundwater–surface water exchanges within a controlled numerical simulation where such exchanges are prevalent in order to evaluate the impact of storage changes on Budyko relationships across a range of spatial scales and climates.

The groundwater contribution ratio map also illustrates the importance of lateral groundwater flow at multiple spatial scales within the system. Groundwater storage gains (i.e., positive values of G/P) are prevalent in the western

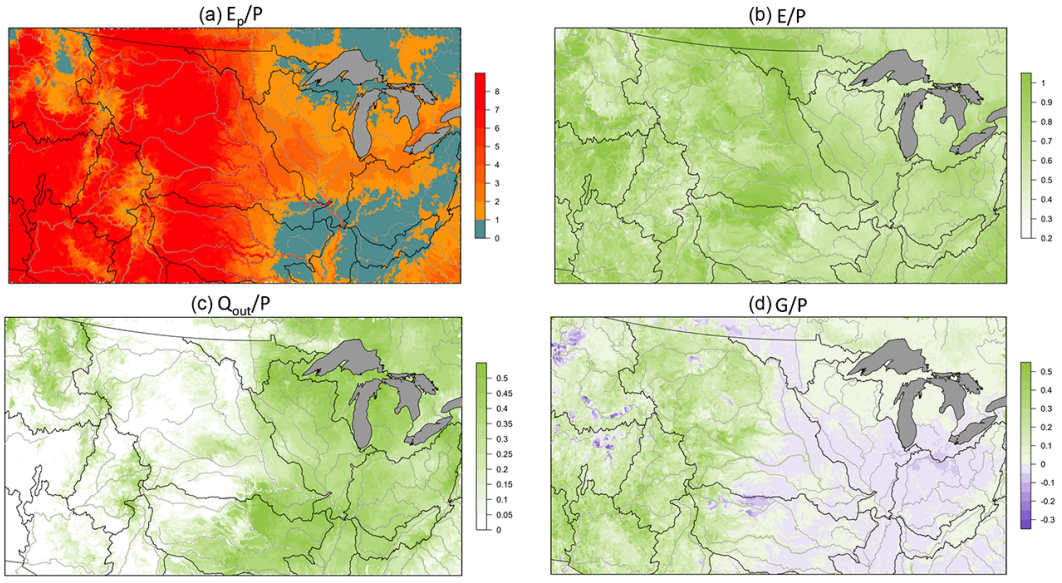

Figure 3. Maps of **(a)** aridity index (E_p/P) and the ratios of **(b)** evapotranspiration, **(c)** outflow and **(d)** groundwater contributions (G/P) compared to precipitation. Major river basins are outlined in black. Note that ratios are mapped according to the subbasins shown in Fig. 2 but the values reflect the water balance for the entire watershed. This is a system of nested watersheds (as illustrated in Fig. 1c) so the value for each watershed is reported at its outlet subbasin.

arid portion of the domain and groundwater discharge to surface water is more common in the humid eastern portion of the domain. Within large basins like the Missouri, positive groundwater contributions occur in the headwater regions and transitions to negative values downstream. This is an illustration of lateral groundwater convergence and regional flow systems. Note that results are mapped by subbasin, but all water balance calculations are carried out for the complete watershed draining to a subbasin outlet. Therefore, Fig. 3 should be viewed as a system of nested subbasins with values representing progressively larger drainage areas as you move downstream (as illustrated in Fig. 1c). With this in mind, it is also intuitive that some of the largest groundwater contribution ratios occur in headwater basins, while in downstream reaches on major rivers the values are smaller, indicating a regional balance between local groundwater–surface water exchanges when aggregating over larger drainage areas.

2.4 Three approaches to evapotranspiration

We have identified three common treatments of evapotranspiration within Budyko analyses. As will be demonstrated later on, these three approaches are identical in systems where the steady-state assumption is valid and no storage changes are occurring. However, when this is not the case, we hypothesize that the different formulations for evapotranspiration will yield systematically different results. Here we summarize the three approaches to E and how each approach is mimicked within the simulated results.

Precipitation and runoff are generally much easier to measure at the watershed scale than evapotranspiration or groundwater storage changes. As a result, in many Budyko analyses evapotranspiration is not actually measured directly, but is calculated as the difference between precipitation and surface outflow (e.g., Greve et al., 2015; Jones et al., 2012; Renner et al., 2014; Wang et al., 2009; Xu et al., 2013; Yang et al., 2009). This approach relies on the assumption that changes in storage are negligible. We refer to this as the *inferred evapotranspiration* approach and mimic it by approximating the evapotranspiration ratio as simulated $(P - Q_{out})/P$. In other words, for this approach, we disregard the simulated evapotranspiration values and generate a new evapotranspiration estimate (i.e., the *inferred evapotranspiration*) indirectly from the precipitation input to the model and the simulated overland flow. To be consistent with other studies, we follow the standard assumption that storage changes are negligible and we do not include groundwater storage changes in this estimate. The implications of this assumption are explored in the results section.

A more direct, if less common, approach is to quantify evapotranspiration from field observations. This approach does not require a steady-state assumption when calculating evapotranspiration but it does require more rigorous field observations and is therefore not feasible for Budyko analysis of data-sparse areas. Within our simulation results, however, "data" is not a limitation. Our modeled outputs include gridded hourly evapotranspiration for the entire domain. Simulated E values are aggregated by watershed and used to represent the so called *direct evapotranspiration*. Note that in

this case we are still using simulated E, not observations. The intention is to treat the model as our synthetic truth and compare variations within this framework.

Finally, the most rigorous, and data-intensive, approach is to quantify both evapotranspiration and groundwater–surface water exchanges directly. This approach has been used in recent studies seeking to evaluate storage impacts on Budyko relationships (e.g., Istanbulluoglu et al., 2012; Wang, 2012). Changes in groundwater storage are not used to adjust evapotranspiration values directly but they can be applied to precipitation estimates to better reflect the quantity of water that is available to partition into overland flow or evapotranspiration. This is defined as effective precipitation and is calculated as precipitation minus groundwater contribution ($P - G$). The effective precipitation approach was used by Du et al. (2016) in their study of Budyko relationships in arid basins. For this study we mimic the effective precipitation approach by using the simulated (or *direct*) evapotranspiration and combining the model input precipitation with the calculated groundwater contributions. The adjustment for effective precipitation within the Budyko framework is covered in Sect. 2.5.

It should be noted here that the first two approaches (i.e., inferred and direct evapotranspiration) are commonly used in analyses that rely on the standard equilibrium assumption while the final method is designed for situations where this is not the case. By comparing results between all three, we consider the impact of nonzero groundwater contributions both for approaches that assume it is negligible and those that account for it.

2.5 Budyko analysis

Budyko's original formulation expressed the evapotranspiration ratio ($E\,/\,P$) as a function of the aridity index (E_p/P) as follows (Budyko, 1974):

$$\frac{E}{P} = \left\{ \frac{E_\mathrm{p}}{P} \left[1 - \exp\left(-\frac{E_\mathrm{p}}{P} \right) \tanh\left(\frac{P}{E_\mathrm{p}} \right) \right] \right\}^{0.5}. \tag{8}$$

Although the original analysis by Budyko did show some scatter around the curve, Eq. (8) defines a universal relationship that does not include any free parameters to account for spatial differences (Budyko, 1974). Subsequent work has observed systematic variability between watersheds that can be related to climate, land cover and soil properties (e.g., Donohue et al., 2007). To reflect this, the original universal Budyko formulation has been refined multiple times to include additional free parameters (Choudhury, 1999; Fu, 1981; Milly, 1994; Zhang et al., 2001, 2004). For a summary of these formulations refer to Du et al. (2016) and Zhang et al. (2004).

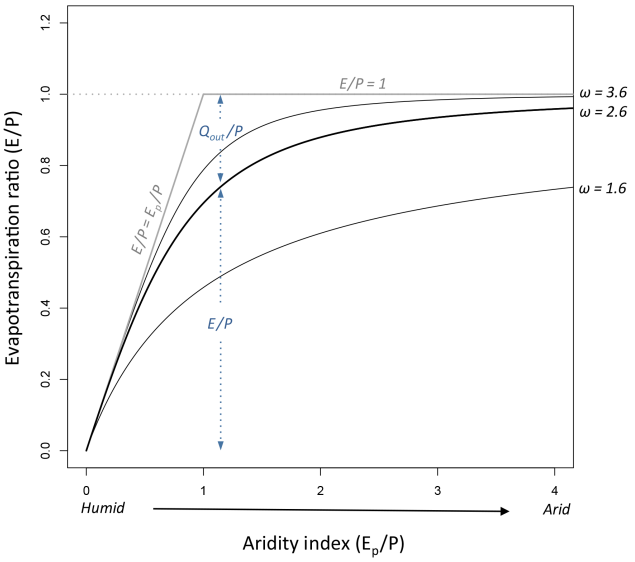

Figure 4. Illustration of the Budkyo framework showing curves with three different shape parameters (black lines, $\omega = 1.6$, 2.6 and 3.6) in relation to the water ($E/P = 1$) and energy ($E/P = E_\mathrm{p}/P$) limits of the system, grey lines.

Here we apply the commonly used Budyko formulation from Fu (1981) and Zhang et al. (2004):

$$\frac{E}{P} = 1 + \frac{E_\mathrm{p}}{P} - \left(1 + \left(\frac{E_\mathrm{p}}{P} \right)^{\omega} \right)^{1/\omega}. \tag{9}$$

Equation (9) includes one free parameter, ω, which can range from 1 to infinity, henceforth referred to as the shape parameter. ω is an empirical parameter that has not been ascribed a specific physical meaning, but is generally conceptualized as an integrated catchment property that reflects characteristics such as land cover, soil properties, topography and seasonality (Zhang et al., 2004). If the evapotranspiration fraction and the aridity index are both known, ω can be calculated for any point on a Budyko plot using Eq. (9).

Figure 4 plots Eq. (8) for a range of ω values. The bold line ($\omega = 2.6$) is roughly equivalent to the original Budyko equation (Eq. 8) (Zhang et al., 2004). Following the original Budyko assumption of there being no change in storage, in humid locations where potential evaporation is less than precipitation, the system is energy-limited and the maximum value of E is E_p. Conversely, when the aridity index is greater than 1 the system is water-limited and the maximum E/P value is 1 (indicating that all incoming precipitation is evaporated). As the shape parameter increases, the curve moves progressively closer to the water ($E/P = 1$) and energy ($E/P = E_\mathrm{p}/P$) limitations of the system.

In the following sections, Budyko relationships are plotted and shape parameters are evaluated for all three approaches using variations of Eq. (9) as follows:

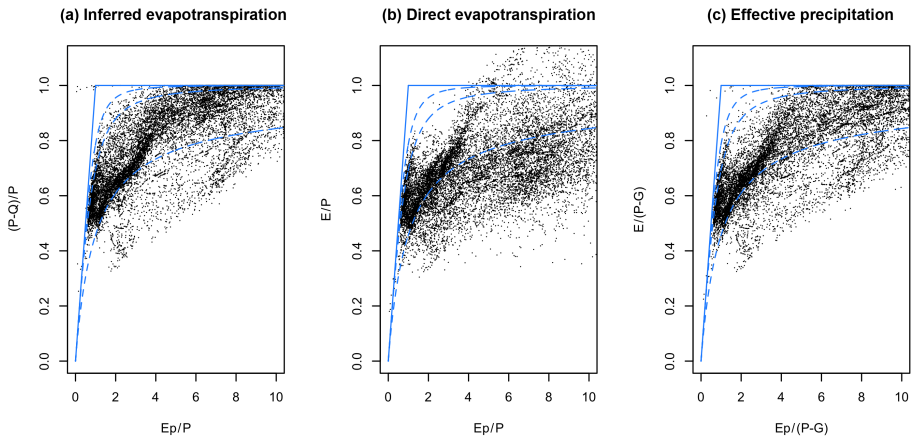

Figure 5. Budyko plots for the three approaches **(a)** inferred evapotranspiration, **(b)** direct evapotranspiration and **(c)** effective precipitation with points for every watershed in the domain. Dashed blue lines are Budyko curves with ω values of 1.6, 2.6 and 3.6 and the solid blue lines are the water and energy limits (refer to Fig. 4).

1. inferred evapotranspiration: evapotranspiration is calculated from precipitation and outflow so $(P - Q_{\text{out}})/P$ is substituted for E/P in Eq. (9);

2. direct evapotranspiration: Eq. (9) is applied as written;

3. effective precipitation: precipitation is replaced by effective precipitation $(P - G)$ which means $E/(P - G)$ replaces E/P and $E_{\text{p}}/(P - G)$ replaces E_{p}/P in Eq. (9).

3 Results and discussion

Results and discussion are divided into two sections. In Sect. 3.1 the three approaches to evapotranspiration fractions are compared across the entire simulation domain. Systematic differences are identified and evaluated as a function of groundwater contributions. A conceptual framework is presented to explain the biases between approaches. In Sect. 3.2 the potential implications of these differences are illustrated by comparing spatial patterns between the three approaches as well as relationships across spatial scales.

3.1 The impact of storage changes on Budyko relationships

Figure 5 plots every watershed in the domain shown in Fig. 2 using the three approaches to estimating the evapotranspiration fraction. In all three figures the watershed points follow the overlaid Budyko curves; 77 % of the watersheds fall within the 1.6 to 3.6 shape parameter lines for the inferred evapotranspiration approach, 51 % for the direct approach and 72 % for the effective precipitation approach. This demonstrates that Budyko relationships are recreated with the integrated hydrologic model. However, there are some notable differences between methods. With the inferred E approach shown in Fig. 5a, the points are focused near the water limit line (i.e., $(P - Q_{\text{out}})/P = 1$) for high aridity values. Conversely, with the direct approach (Fig. 5b), the evapotranspiration ratios are generally lower at high aridity values. Also, with the direct approach, there are points with evapotranspiration ratios greater than 1 and which fall above the water limit. This would appear to violate the water balance and will be discussed more later. There are also a small number of points (less than 20) in Fig. 5a and c that fall to the left of the energy limit line; this behavior results from the treatment of atmospheric stability in the E_{p} calculation.

Systematic differences between the Budyko plots shown in Fig. 5 are explained by the way groundwater contributions influence each approach. This is illustrated conceptually in Fig. 6. In systems with groundwater–surface water interactions, incoming precipitation is equal to the sum of evapotranspiration, outflow and ground water contributions (Eq. 6). This means that the difference between precipitation and outflow will only equal evapotranspiration if there are no storage changes (i.e., G is zero); if there are non-zero groundwater contributions then precipitation minus outflow is actually a measure of evapotranspiration plus groundwater contributions (and not the intended evapotranspiration). In other words, instead of evaluating

$$\frac{E}{P} = f\left(\frac{E_{\text{p}}}{P}\right) \tag{10}$$

as intended in the Budyko formulation, the inferred evapotranspiration approach shown in Fig. 5a is actually plotting

$$\left(\frac{E}{P} + \frac{G}{P}\right) = f\left(\frac{E_{\text{p}}}{P}\right). \tag{11}$$

This is illustrated in Fig. 6a; the curve is now plotting the sum of the evapotranspiration fraction and the groundwater contribution fraction, not the evapotranspiration fraction for

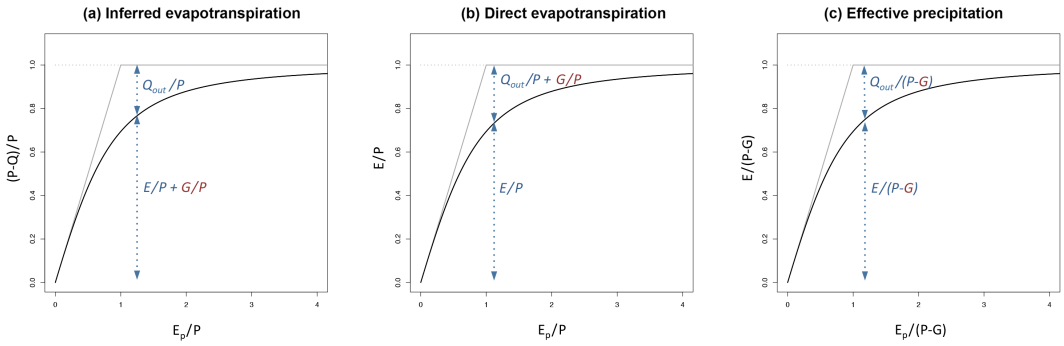

Figure 6. Illustration of the treatment of groundwater contributions for each of the three approaches. The black lines show the water and energy limits and an example Budyko curve, similar to Fig. 4. Arrows indicate the water balance component represented above and below the curve in each case.

the original formulation shown in Fig. 4. The difference between the curve and the limit lines in this case is, however, still the outflow fraction.

The direct evapotranspiration approach avoids the limitations of the inferred approach by evaluating Budyko relationships as a function of the evapotranspiration fraction as intended in Eq. (10). However, groundwater contributions will still bias the results with this approach because the difference between precipitation and evapotranspiration is outflow plus groundwater contribution (Eq. 6). Thus, the curve in Fig. 6b represents the evapotranspiration fraction (as with Fig. 4) but now the partitioning is occurring between evaporation and runoff plus groundwater contributions, not just runoff. This means that the maximum evapotranspiration fraction (i.e., the upper water limit) is not 1, but 1 minus the groundwater contribution fraction.

This shift in the upper limits of water availability explains the values greater than 1 in Fig. 5b; in these watersheds groundwater contributions are negative (i.e., groundwater is supplying water to the land surface) and this allows for evapotranspiration values that are greater than the incoming precipitation. Similar shifts in the upper limits of the system for arid locations were found by Potter and Zhang (2009) who noted that evapotranspiration was actually approaching a fixed portion of potential evapotranspiration for high-rainfall years in arid basins in Australia.

The effective precipitation approach is designed to maintain focus on partitioning between evapotranspiration and overland flow by removing groundwater contributions from the denominator of both ratios (i.e., adjusting both the x and y axes in Fig. 6c) . This ensures that the modified outflow and evapotranspiration ratios will sum to 1 even when groundwater–surface water exchanges are occurring; to accomplish this the modified ratios are expressed as a function of effective precipitation, not precipitation. It should also be noted from Fig. 6 that in the case where G is zero (i.e., there are no storage changes), the three formulations are equivalent.

The systematic differences explained in Fig. 6 are evaluated by calculating the shape parameter (Eq. 9) for the curve corresponding to every watershed plotted in Fig. 5. Figure 7a–c plot the resulting shape parameters as a function of groundwater contribution fraction colored by aridity for each of the three approaches. Recall from Fig. 4 that larger curve numbers fall closer to the upper limits on the Budyko plots and positive groundwater contribution fractions occur when there is a net flux from the surface water to the groundwater (i.e., net infiltration). Positive G values are most prevalent in the more arid western portions of the domain as is shown in Fig. 3d and demonstrated by the shading in Fig. 7a–c where the most, red (arid) points occur further to the right along the x axis. As would be expected from Fig. 6, Fig. 7a–c illustrate varying relationships between shape parameters and groundwater contributions for the different approaches. Recall that all of the results are based on the same underlying simulation so the differences in Fig. 7 result purely from accounting differences in how the evapotranspiration fraction is calculated between approaches.

Both the inferred (Fig. 6a) and direct approaches (Fig. 6b) show clear, but contradictory, relationships with groundwater–surface water exchanges. There is a positive relationship between the shape parameter and groundwater contribution fraction for the inferred evapotranspiration approach at the lower limits of the system, as delineated by the dashed line in Fig. 7a. This indicates that in arid watersheds, increased groundwater contributions are correlated with larger evapotranspiration fraction (i.e., with larger curve numbers). This behavior is consistent with Fig. 6a; because the groundwater contribution is included in the evapotranspiration fraction when evapotranspiration is inferred from precipitation and outflow (i.e., $P - Q_{\text{out}} = E + G$), nonzero groundwater contributions vertically shift points in the Budyko plot.

Taking this idea further, Fig. 7d shows that a constant positive groundwater contribution applied across aridity values will vertically shift the Budyko curve relative to a scenario with no storage changes if evapotranspiration is inferred. In

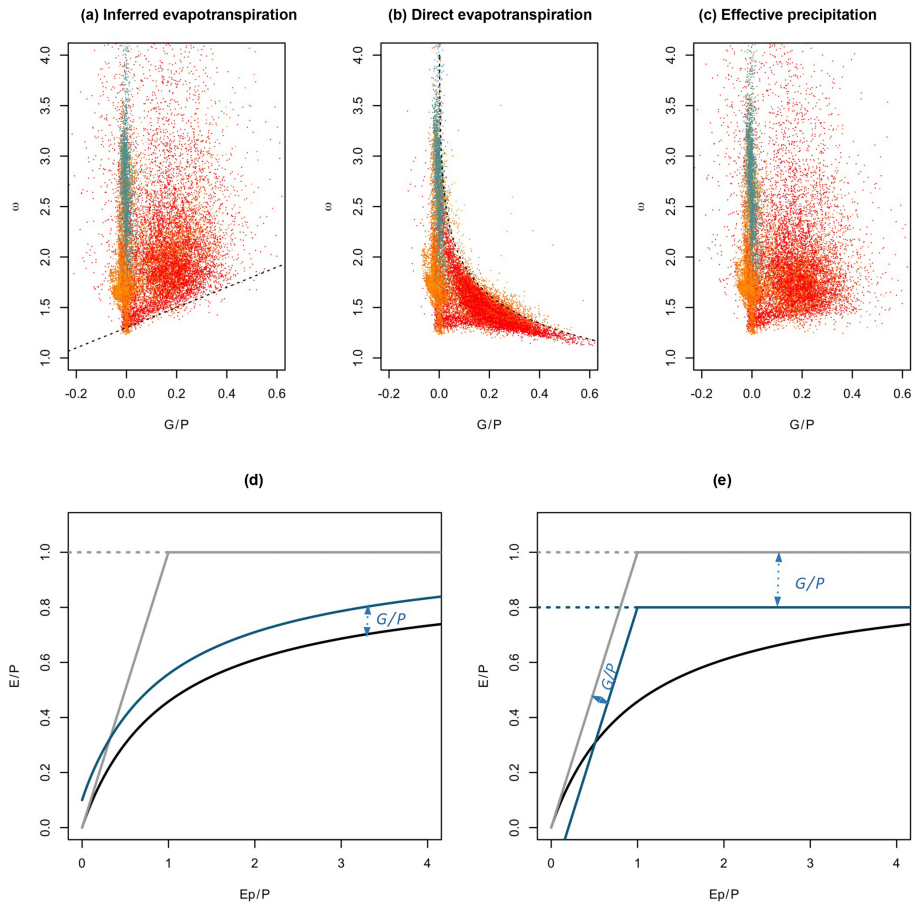

Figure 7. Comparison of shape parameters to groundwater contribution ratios for the three approaches in every watershed **(a–c)**. Points are colored by aridity as shown in Fig. 3a. A dashed line with a slope of 1 is included on **(a)** for reference. The dashed line on **(b)** shows the relationship between the shape parameter and groundwater contribution fraction for an example aridity value of 6 in the limiting case where outflow is zero. The conceptual figures below illustrate the impact of a positive groundwater contribution (i.e., a net flux from the surface to the subsurface) for **(d)** the inferred evapotranspiration and **(e)** direct evapotranspiration approaches.

the case of a positive groundwater contribution, this vertical shift moves points closer to the water and energy limits of the system, and therefore increases their shape parameters. Note that in the Fu equation (Eq. 9), Budyko curves with different shape parameter are not parallel to one another and converge at low aridity values; therefore the same groundwater contribution value changes the shape parameter differently depending on the location within the Budyko plot. The linear trend traced along the lower portion of the scatter plot in Fig. 7a shows that for the lowest curve numbers, occurring in watersheds with high aridity, there is a roughly linear relationship between groundwater contribution and shape parameters. This approximate linearity occurs because the Fu curves become almost parallel for high aridity values (see Fig. 4). For lower aridity values, this is not the case and the relationship between groundwater contribution and shape parameter will be positive but nonlinear.

Figure 7b plots groundwater contributions versus shape parameters similar to Fig. 6a but for the direct evapotranspiration approach. Recall that with this approach the groundwater contributions are now essentially lumped with the outflow fraction (as opposed to the evapotranspiration fraction with the inferred approach; refer to Fig. 6a and b). This means that rather than shifting points vertically in the Budyko plot (i.e., Fig. 7d), positive groundwater contributions change the total water that is available for evapotranspiration. This can be conceptualized as shifting the limits of how much total water is available for evapotranspiration.

In this case a positive groundwater contribution (i.e., surface water infiltrating to groundwater) is essentially a loss to the surface water system and decreases the upper limit of water available. Figure 7e illustrates this point for a constant groundwater contribution across the entire Budyko plot. When groundwater contributions are present, the upper water limitation on the system shifts from 1 to $1 - G/P$ and the energy limitation shifts from E_p/P to $E_p/P - G/P$. However, if different watersheds have varying levels of groundwater contribution, this means that each watershed will now have a

different upper limit; in other words, the evapotranspiration fraction plus the outflow fraction is no longer always equal to 1 but rather 1 minus the groundwater contribution fraction. This creates a nonlinear inverse relationship between curve number and groundwater contributions. As the groundwater contribution fraction increases, the decreasing upper bounds on evapotranspiration fraction will bias the system towards lower curve numbers (refer to Fig. 4). This is a nonlinear relationship which can be shown by calculating the shape parameter as a function of groundwater contribution fraction in Eq. (9) for the limiting case where there is no outflow (i.e., $G/P = 1 - E/P$). The dashed line in Fig. 7b shows the resulting relationship for a relatively high aridity value of 6. The curve provides a good approximation for the upper limit of Fig. 6b.

Finally, a scatter plot of shape parameters versus groundwater contribution fraction for the effective precipitation case (Fig. 6c) shows similar patterns with aridity but no clear correlation between storage changes and shape parameters. This is to be expected because the effective precipitation approach adjusts for groundwater contributions in both the evapotranspiration ratios and the aridity index before plotting. However, it should be noted that some dependence on groundwater contribution is still to be expected, to the extent that groundwater–surface water exchanges are also correlated with other watershed properties. For example, groundwater contribution levels can also be correlated with vegetation type, soil properties and other watershed characteristics, which have been correlated to shape parameters in previous research (e.g., Li et al., 2013; Shao et al., 2012; Williams et al., 2012; Xu et al., 2013; Yang et al., 2009).

This is true for the other approaches too; while the effect of groundwater contributions within each space can be precisely determined using Eqs. (7) and (9), it is important to note that the watersheds evaluated here are also heterogeneous in land cover, topography and seasonality. Therefore, in the scatter plots shown in Fig. 7, the relationships between shape parameters and groundwater contribution explained by Fig. 7d and e appear as limits rather than strong predictors. This point is also made by Istanbulluoglu et al. (2012) who evaluated the impact of groundwater storage changes on Budyko relationships using the inferred evapotranspiration approach and adjusting for storage changes using estimates from groundwater observations. They provide a similar conceptual model to Fig. 7d, describing consistent shifts within the Budyko space as a function of groundwater contribution. However, for the four basins in Nebraska that they evaluated they found a negative relationship between inferred evapotranspiration ratios and aridity. This was attributed to a strong negative correlation between groundwater contribution fraction and aridity index. In other words, for this subset of basins, they show that the resulting trend is controlled by the dependence of groundwater contribution on other watershed characteristics.

Figure 8 compares the shape parameters calculated with each approach to illustrate the way that different assumptions can bias derived Budyko relationships. Figure 8a shows the differences between the inferred and direct evapotranspiration approaches, which are commonly used in studies that assume no change in storage. Because groundwater contributions are incorporated into different components of the water balance with these methods, Fig. 8a shows that, for positive groundwater contributions (green points), the inferred shape parameters are systematically higher than the direct shape parameters, while the inverse is true when groundwater contributions are negative (purple points). Furthermore, when groundwater contributions are large (i.e., the dark green circles in Fig. 8a), the direct method has uniformly low shape parameters, but the inferred method still shows a range of shape parameters. This is to be expected from the conceptual model of the direct evapotranspiration approach (Fig. 7e), where we showed that high groundwater contributions decrease the upper limit of the evapotranspiration ratio. This shift biases the system towards uniformly low shape parameters that are less sensitive to other watershed characteristics.

The direct and inferred evapotranspiration methods are also compared to the effective precipitation approach, which does account for groundwater contributions (Fig. 7b and c). As would be expected, the direct and inferred approaches have inverse biases relative to the effective precipitation method; shape parameters are systematically higher with the inferred approach relative to effective precipitation and lower for the direct approach. Here too, the trends with groundwater contributions are reversed, with positive contributions creating a positive bias for the inferred case and a negative bias for the effective precipitation case. This result is in keeping with the conceptual model of groundwater contributions to each approach; with the inferred evapotranspiration approach, groundwater contributions are lumped with evapotranspiration, while in the direct approach they are lumped with outflows.

Also, there is a much stronger correlation between the inferred evapotranspiration and effective precipitation approaches (Fig. 8b) than between direct evapotranspiration and effective evapotranspiration approaches (Fig. 8c) (r^2 value of 0.96 comparing inferred versus effective as opposed to 0.32 for inferred versus direct). This is partially due to the lack of sensitivity of shape parameters in the direct approach when groundwater contributions are large, as was previously noted and is also illustrated in Fig. 8a. For all three cases, Fig. 8 demonstrates systematic variability in the shape parameter even for relatively small groundwater contributions. As with Fig. 7, in Fig. 8 there is still significant scatter in each of these comparisons. In this case the scatter is caused by the fact that the shape parameter will be impacted (1) by how large the groundwater contribution fraction is and (2) the aridity of the watershed. Groundwater contributions shift points within the Budyko plot in a linear fashion (although the direction varies according to the approach) but

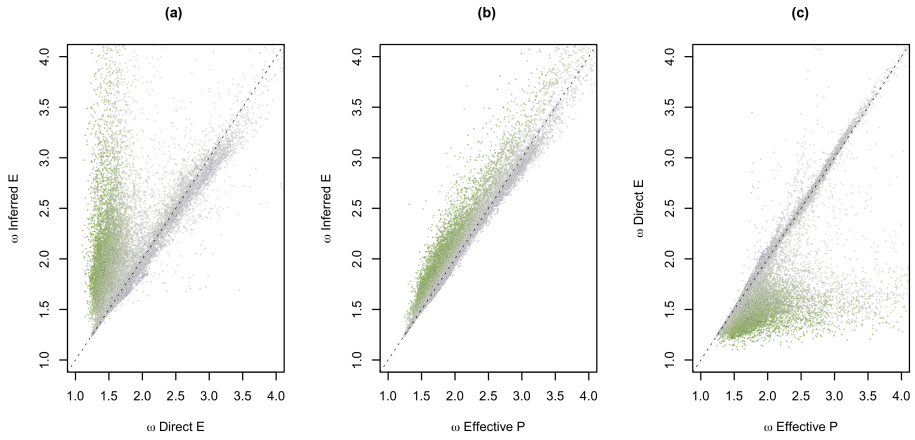

Figure 8. Comparison of shape parameters between the three approaches for every watershed. Points are colored by groundwater contribution fraction as shown in Fig. 3d. The dashed line on each plot is a one-to-one line for reference.

the resulting change in shape parameter will have a nonlinear dependence on both aridity and evapotranspiration fraction.

3.2 Spatial patterns and scaling

Section 3.1 explored the relationship between groundwater storage and shape parameters using the three different approaches to evapotranspiration fractions. Here, we illustrate the impacts of these differences on spatial patterns in shape parameters and scaling relationships. The intent is to provide a demonstration of how systematic differences will propagate across spatial scales using the 1985 simulation as a test case. Obviously local differences will vary depending on the time period used for analysis and the associated levels of groundwater contribution.

Figure 9 maps shape parameters for all of the roughly 25 000 nested watersheds in the simulation domain, calculated using the three different approaches to evapotranspiration ratios. Even though the 1-year transient simulation used for the analysis presented does not meet the Budyko equilibrium criteria, Figs. 4c and 8c show that realistic Budyko relationships are still found when groundwater contributions are accounted for using the effective precipitation approach. Xu et al. (2013) built a neural network model to predict shape parameters using long-term observations from 224 watersheds with drainage areas ranging from 100 to 10 000 km^2. They then predicted shape parameters globally using a variety of catchment characteristics. Excluding the small drainage areas with shape parameters greater than four, the spatial patterns calculated here with the effective precipitation approach (i.e., the only approach that corrects for groundwater contributions, Fig. 9c) match well with the global map presented by Xu et al. (2013).

All three maps demonstrate local variability and regional trends in the shape parameters. This spatial variability is partially caused by the spatial patterns in groundwater contribution fraction shown in Fig. 3d; however, it is also a reflection

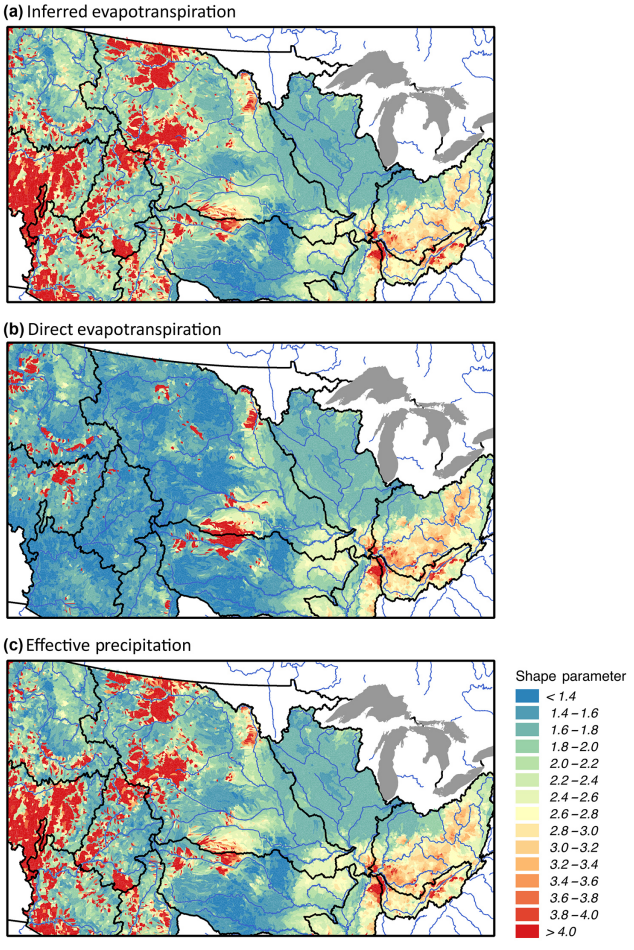

Figure 9. Map of shape parameters calculated for the 24 235 nested watersheds using the **(a)** inferred evapotranspiration, **(b)** direct evapotranspiration and **(c)** effective precipitation. Major rivers are outlined in blue and regional boundaries in black.

of variability in catchment characteristics such as vegetative properties, topography and climate that have been correlated to Budyko relationships by previous studies (e.g., Li et al., 2013; Milly, 1994; Shao et al., 2012; Williams et al., 2012; Xu et al., 2013; Yang et al., 2009; Yokoo et al., 2008). The purpose here is not to isolate all of the sources of spatial heterogeneity, but rather to illustrate how spatial patterns change depending on the treatment of storage.

Spatial patterns are consistent between the three approaches in the more humid eastern portion of the domain, where groundwater contribution ratios are generally smaller (Fig. 3d), but in the more arid western portion of the domain significant differences are observed. For both the inferred evapotranspiration and effective precipitation approaches there are large red areas indicating shape parameters greater than four where the evapotranspiration ratio is falling very close to the water limitation. The areas with the highest shape parameters (i.e., greater than four) are generally consistent between the inferred evapotranspiration and effective precipitation approaches, but the inferred approach results in higher curve numbers throughout the western portion of the domain than the effective precipitation approach. This is consistent with Fig. 8b, which showed strong correlations between the shape parameters of these two approaches ($r^2 = 0.96$) but a slight positive bias with positive groundwater contributions for the inferred evapotranspiration approach; 62 % of watersheds overall and 86 % of watersheds with a positive groundwater contribution have a higher shape parameter using the inferred evapotranspiration approach.

Conversely, with the direct evapotranspiration approach, the western portion of the domain has much lower shape parameters and less spatial variability. Again, this finding is consistent with Fig. 7b and e, which show that when groundwater contributions are high, the curve numbers are uniformly low because the flux from the surface water system to the groundwater shifts the upper limit of the evapotranspiration fraction down. The systematic differences in Fig. 9, both with respect to the shape parameter values and the spatial patterns in these parameters, where groundwater–surface water exchanges are occurring indicate the potential to arrive at fundamentally different conclusions about spatial trends in shape parameters, depending on the approach used.

Next, we evaluate groundwater impacts as a function of drainage area. Budyko originally limited analysis to large basins (which he defined as drainage areas greater than 10 000 km^2) where he argued that macroclimate can be expected to dominate partitioning (Budyko, 1974). Indeed subsequent work has shown that for smaller areas vegetation dynamics become increasingly important (Donohue et al., 2007). Figure 10 plots Budyko relationships for every watershed grouped by drainage area using the effective precipitation formulation as an example. In this figure, the drainage area is increased from watersheds less than 1000 km^2 (Fig. 9a) to watersheds greater than 100 000 km^2 (Fig. 9d). This figure shows that the scatter decreases as drainage area increases and the points converge around a single curve. This behavior illustrates increased importance of local watershed characteristics for smaller drainage areas consistent with previous studies (e.g., Budyko, 1974; Donohue et al., 2007). We do not show the other two approaches for this example because similar convergence behavior with larger drainage areas is found in all three cases.

The shape parameters estimated with the effective precipitation approach are arguably the most comparable to other long-term studies that have assumed equilibrium conditions (assuming that the watersheds they studied actually were in equilibrium over the study period). The simulated median value found here is slightly lower than the original Budyko value of 2.6 and the median value of 2.56 found by Greve et al. (2015) using the 411 Model Parameter Estimation Experiment (MOPEX) catchments in the US. However, it compares well with 1.8 median value for large MOPEX basins in the US reported by Xu et al. (2013); although, it should be noted that Xu et al. (2013) report a higher 2.6 median value for small basins, and the median small basin value reported here is 2.0. Part of this bias can likely be attributed to the concentration of MOPEX basins in the eastern portion of the US where Fig. 9 shows that shape parameters are generally higher. Overall, the consistency in spatial patterns and convergence around the Budyko curve for large drainage areas indicates that the ParFlow–CLM model recreates Budyko relationships even over a relatively short annual simulation period, as long as groundwater contributions are adjusted for (i.e., using the effective precipitation approach). However, for smaller watersheds, variability in catchment characteristics is still an important consideration.

While all three approaches have decreased variance with increased drainage area, the median and variance are not necessarily consistent between methods. Figure 11 shows the interquartile range of shape parameters for each approach with increasing drainage area. In all three cases, the 75th percentile shape parameters decrease and the 25th percentile shape parameter increases with increasing area. Again this indicates increased importance of watershed characteristics at smaller scales; local variability is muted and the probability of observing very high or very low shape parameters decreases as the scale increases from smaller to larger watersheds. In the case of the inferred and direct evapotranspiration approaches, because groundwater contributions are not accounted for in the calculations, some of this variability can also be attributed to spatial patterns in groundwater–surface water exchanges and lateral groundwater flow. As previously noted, the groundwater contribution map (Fig. 3d) shows that the largest (positive or negative) groundwater contribution fractions generally occur in small headwater basins. Across larger areas, local groundwater–surface water exchanges balance out and the overall groundwater contribution fractions for large watersheds tend to be smaller.

Consistent with Figs. 7 and 8, the inferred evapotranspiration and effective precipitation approaches are the most simi-

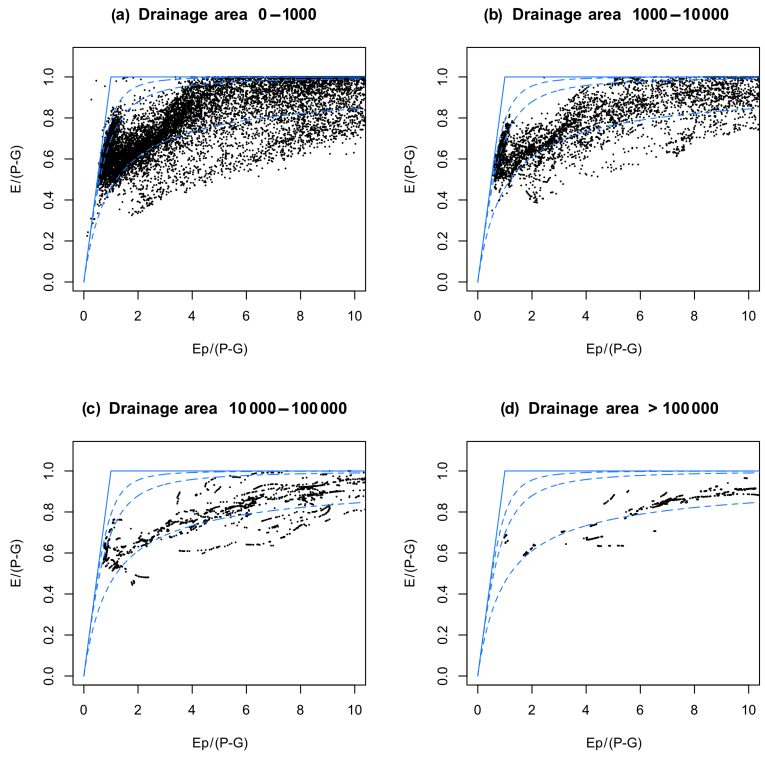

Figure 10. Budyko plots of evapotranspiration ratio versus aridity index using the effective precipitation method with watersheds grouped by drainage area [km^2]. Blue dashed lines are Budyko curves with shape parameters of 1.6, 2.6 and 3.6 (refer to Fig. 4) and the solid blue lines show the water and energy limits.

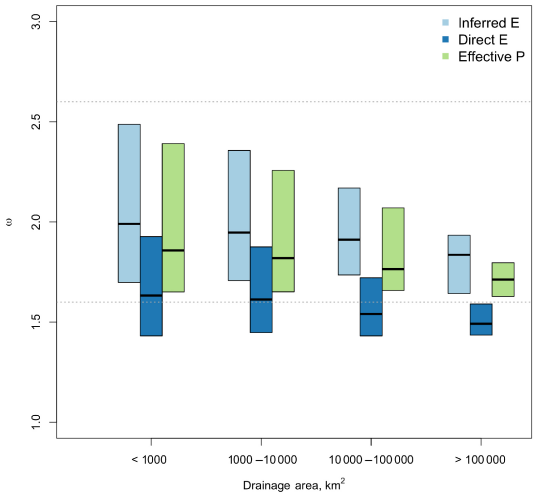

Figure 11. Box plots showing the interquartile range (i.e., 25–75th percentile values) of shape parameters for all three approaches grouped by drainage area. Dashed lines are at 1.6 and 2.6 for reference.

lar. For the largest drainage areas, the median shape parameter is 1.8 for the inferred evapotranspiration approach, 1.5 for the direct evapotranspiration approach and 1.7 using effective precipitation. The direct evapotranspiration formulation has systematically lower shape parameters than the other two approaches; the median value for this method is consistently below the other two. Again this agrees with Sect. 3.1 where we demonstrated an inverse relationship between shape parameters and groundwater contributions. The direct evapotranspiration approach also has a consistently smaller interquartile range than the other two methods. This results from the negative correlation with groundwater contribution and the decreased sensitivity that was shown for small shape parameters in arid locations. Figure 11 shows that all three approaches will yield qualitatively similar scaling relationships and convergence for large basins; however, the shape parameter values will vary.

4 Conclusions

One of the primary assumptions of the Budyko hypothesis is that watersheds are in equilibrium and there are no changes in storage. This means that all incoming precipitation will either leave the watershed as evapotranspiration or overland flow. While the original Budyko curve has been well verified with observations from around the globe, it is also now widely accepted that the relationship between evapotranspiration ratios and aridity indices is not universal, and some additional curve parameters are needed to account for spa-

tial variability between watersheds. Many subsequent studies have related curve parameters to catchment properties such as vegetation, topography and seasonality (e.g., Li et al., 2013; Shao et al., 2012; Williams et al., 2012; Xu et al., 2013; Yang et al., 2009). More recently, additional studies have shown that if groundwater–surface water exchanges are present this can also influence the shape of the curve and account for additional variability between watersheds (Milly and Dunne, 2002; Zhang et al., 2008).

While methods have been developed to account for storage changes within the Budyko framework (e.g., Du et al., 2016), very few studies have sufficient data on groundwater–surface water interactions to evaluate the validity of the equilibrium assumption, much less to precisely quantify storage changes in their analysis. One of the key advantages of the Budyko approach is its ability to predict behavior based on a small number of relatively easy-to-obtain observations. Given its common application to data-sparse watersheds, where even evapotranspiration measurements are often not available, directly quantifying groundwater–surface water exchanges in these locations seems unlikely. Therefore, it is important to understand the sensitivity of Budyko relationships to uncertainty in storage changes in a general context that can be used to interpret results where precise measurements are not available.

Previous work has demonstrated systematic shifts in Budyko plots caused by groundwater–surface water interactions (Du et al., 2016; Istanbulluoglu et al., 2012; Milly and Dunne, 2002; Wang, 2012; Zhang et al., 2004). Here we demonstrate that the influence of groundwater storage changes on Budyko results will vary depending on how evapotranspiration is handled in the study. If evapotranspiration is measured directly, positive groundwater contributions (i.e., net infiltration from the surface to the subsurface) shift shape parameters down; conversely, if evapotranspiration is estimated using precipitation and runoff, positive groundwater contributions will increase shape parameters. In both cases the sensitivity of the shape parameter to storage changes varies non-linearly with both the aridity of the watershed and the evapotranspiration fraction.

Using a 1-year simulation with an integrated hydrologic model, we demonstrate these differences can result in different conclusions about spatial patterns in Budyko relationships and the median shape parameter across spatial scales. This indicates that it is important to consider the approach used for estimating evapotranspiration fractions when comparing results between studies, and provides a demonstration of the types of bias that would be expected if different methods are used.

These results also have implications for the myriad of studies that seek to relate shape parameters for Budyko curves to other watershed characteristics. The conceptual models shown here illustrate that groundwater contributions will shift points in consistent and predictable ways when other variables are held constant (i.e., if you apply a consistent groundwater contribution across the entire range of aridity values or consider the shift of a single point with a given aridity value). However, we use the results from our integrated hydrologic model to demonstrate that, within complex heterogeneous domains, groundwater–surface water exchanges are spatially heterogeneous and depend on watershed characteristics such as aridity values, which can also influence Budyko relationships. The scatter in Figs. 6 and 7 demonstrates that groundwater contributions cannot easily serve as an independent predictor of the shape of Budyko relationships. This also shows that in large comparative studies, the bias caused by groundwater–surface water interactions may not be readily apparent because it will vary from watershed to watershed.

The intention of these comparisons is not to discredit previous approaches, but rather to illustrate the potential impacts of assuming equilibrium conditions across a broad range of physiographic settings and spatial scales without the ability to verify this assumption. Our results show that even when changes in storage are occurring, large watersheds still roughly follow the Budyko curve; however, the shape parameter and scatter will vary with groundwater contribution and depending on how evapotranspiration is quantified. We suggest that studies that cannot verify the equilibrium assumption using groundwater observations include additional analysis to evaluate the sensitivity of their findings to uncertainty in storage changes by perturbing points using the conceptual models presented here. Even if groundwater contributions cannot be directly incorporated into analyses, this can help determine whether differences in shape parameters are actually resulting from unique basin characteristics or uncertainty in storage.

5 Data availability

All data from this analysis are available upon request. Instructions for accessing the ParFlow simulations used here are provided in Maxwell and Condon (2016).

Competing interests. The authors declare that they have no conflict of interest.

Acknowledgements. Funding for this work was provided by the US Department of Energy Office of Science, Offices of Advanced Scientific Computing Research and Biological and Environmental Sciences IDEAS project. The ParFlow simulations were also made possible through high-performance computing support from Yellowstone (ark:/85065/d7wd3xhc) provided by National Center for Atmospheric Research's Computational and Information Systems Laboratory, sponsored by the National Science Foundation.

Edited by: M. Bierkens
Reviewed by: four anonymous referees

References

Barnes, M. L., Welty, C., and Miller, A. J.: Global Topographic Slope Enforcement to Ensure Connectivity and Drainage in an Urban Terrain, J. Hydrol. Eng., 21, 06015017, doi:10.1061/(ASCE)HE.1943-5584.0001306, 2016.

Budyko, M. I.: The Heat Balance of the Earth's Surface Rep., US Department of Commerce, Weather Bureau, Washington, D.C., 140–161, 1958.

Budyko, M. I.: Climate and LIfe, Academic Press, New York, 1974.

Choudhury, B.: Evaluation of an empirical equation for annual evaporation using field observations and results from a biophysical model, J. Hydrol., 216, 99–110, doi:10.1016/S0022-1694(98)00293-5, 1999.

Condon, L. E., Hering, A. S., and Maxwell, R. M.: Quantitative assessment of groundwater controls across major US river basins using a multi-model regression algorithm, Adv. Water Resour., 82, 106–123, doi:10.1016/j.advwatres.2015.04.008, 2015.

Cosgrove, B. A., Lohmann, D., Mitchell, K. E., Houser, P. R., Wood, E. F., Schaake, J. C., Robock, A., Marshall, C., Sheffield, J., Duan, Q., Luo, L., Higgins, R. W., Pinker, R. T., Tarpley, J. D., and Meng, J.: Real-time and retrospective forcing in the North American Land Data Assimilation System (NLDAS) project, J. Geophys. Res., 108, 8842, doi:10.1029/2002JD003118, 2003.

Dai, Y., Zeng, X., Dickinson, R. E., Baker, I., Bonan, G. B., Bosilovich, M. G., Denning, A. S., Dirmeyer, P. A., Houser, P. R., Niu, G., Oleson, K. W., Schlosser, C. A., and Yang, Z.-L.: The Common Land Model, B. Am. Meterorol. Soc., 84, 1013–1023, doi:10.1175/BAMS-84-8-1013, 2003.

Donohue, R. J., Roderick, M. L., and McVicar, T. R.: On the importance of including vegetation dynamics in Budyko's hydrological model, Hydrol. Earth Syst. Sci., 11, 983–995, doi:10.5194/hess-11-983-2007, 2007.

Donohue, R. J., Roderick, M. L., and McVicar, T. R.: Assessing the differences in sensitivities of runoff to changes in climatic conditions across a large basin, J. Hydrol., 406, 234–244, doi:10.1016/j.jhydrol.2011.07.003, 2011.

Du, C., Sun, F., Yu, J., Liu, X., and Chen, Y.: New interpretation of the role of water balance in an extended Budyko hypothesis in arid regions, Hydrol. Earth Syst. Sci., 20, 393–409, doi:10.5194/hess-20-393-2016, 2016.

Ferguson, I. M., Jefferson, J. L., Maxwell, R. M., and Kollet, S. J.: Effects of root water uptake formulation on simulated water and energy budgets at local and basin scales, Environ. Earth Sci., 75, 1–15, doi:10.1007/s12665-015-5041-z, 2016.

Fu, B. P.: On the calculation of the evaporation from land surface, Sci. Atmos. Sin., 5, 23–31, 1981.

Gentine, P., D'Odorico, P., Lintner, B. R., Sivandran, G., and Salvucci, G.: Interdependence of climate, soil, and vegetation as constrained by the Budyko curve, Geophys. Res. Lett., 39, L19404, doi:10.1029/2012GL053492, 2012.

Gleeson, T., Smith, L., Moosdorf, N., Hartmann, J., Durr, H. H., Manning, A. H., van Beek, L. P. H., and Jellinek, A. M.: Mapping permeability over the surface of the Earth, Geophys. Res. Lett., 38, L02401, doi:10.1029/2010GL045565, 2011.

Greve, P., Gudmundsson, L., Orlowsky, B., and Seneviratne, S. I.: Introducing a probabilistic Budyko framework, Geophys. Res. Lett., 42, 2261–2269, doi:10.1002/2015GL063449, 2015.

Istanbulluoglu, E., Wang, T., Wright, O. M., and Lenters, J. D.: Interpretation of hydrologic trends from a water balance perspective: The role of groundwater storage in the Budyko hypothesis, Water Resour. Res., 48, W00H16, doi:10.1029/2010WR010100, 2012.

Jefferson, J. L. and Maxwell, R. M.: Evaluation of simple to complex parameterizations of bare ground evaporation, J. Adv. Model. Earth Syst., 7, 1075–1092, doi:10.1002/2014MS000398, 2015.

Jones, J. A., Creed, I. F., Hatcher, K. L., Warren, R. J., Adams, M. B., Benson, M. H., Boose, E., Brown, W. A., Campbell, J. L., and Covich, A.: Ecosystem processes and human influences regulate streamflow response to climate change at long-term ecological research sites, BioScience, 62, 390–404, 2012.

Kollet, S. J. and Maxwell, R. M.: Integrated surface–groundwater flow modeling: A free-surface overland flow boundary condition in a parallel groundwater flow model, Adv. Water Resour., 29, 945–958, doi:10.1016/j.advwatres.2005.08.006, 2006.

Kollet, S. J. and Maxwell, R. M.: Capturing the influence of groundwater dynamics on land surface processes using an integrated, distributed watershed model, Water Resour. Res., 44, W02402, doi:10.1029/2007WR006004, 2008.

Koster, R. D. and Suarez, M. J.: A Simple Framework for Examining the Interannual Variability of Land Surface Moisture Fluxes, J. Climate, 12, 1911–1917, doi:10.1175/1520-0442(1999)012<1911:ASFFET>2.0.CO;2, 1999.

Li, D., Pan, M., Cong, Z., Zhang, L., and Wood, E.: Vegetation control on water and energy balance within the Budyko framework, Water Resour. Res., 49, 969–976, doi:10.1002/wrcr.20107, 2013.

Maxwell, R. M.: A terrain-following grid transform for parallel, large-scale, integrated hydrologic modeling, Adv. Water Resour., 53, 109–117, doi:10.1016/j.advwatres.2012.10.001, 2013.

Maxwell, R. M. and Condon, L. E.: Connections between groundwater flow and transpiration partitioning, Science, 353, 377–380, doi:10.1126/science.aaf7891, 2016.

Maxwell, R. M. and Miller, N. L.: Development of a coupled land surface and groundwater model, J. Hydrometerol., 6, 233–247, doi:10.1175/JHM422.1, 2005.

Maxwell, R. M., Condon, L. E., and Kollet, S. J.: A high-resolution simulation of groundwater and surface water over most of the continental US with the integrated hydrologic model ParFlow v3, Geosci. Model Dev., 8, 923–937, doi:10.5194/gmd-8-923-2015, 2015.

Maxwell, R. M., Condon, L. E., Kollet, S. J., Maher, K., Haggerty, R., and Forrester, M. M.: The imprint of climate and geology on the residence times of groundwater, Geophys. Res. Lett., 43, 701–708, doi:10.1002/2015GL066916, 2016.

Milly, P. C. D.: Climate, soil water storage, and the average annual water balance, Water Resour. Res., 30, 2143–2156, doi:10.1029/94WR00586, 1994.

Milly, P. C. D. and Dunne, K. A.: Macroscale water fluxes 2. Water and energy supply control of their interannual variability, Water Resour. Res., 38, 24-21–24-29, doi:10.1029/2001WR000760, 2002.

Mitchell, K. E., Lohmann, D., Houser, P. R., Wood, E. F., Schaake, J. C., Robock, A., Cosgrove, B. A., Sheffield, J., Duan, Q., Luo, L., Higgins, R. W., Pinker, R. T., Tarpley, D. J., Lettenmaier, D. P., Marshall, C. H., Entin, J. K., Pan, M., Shi, W., Koren, V., Meng, J., Ramsay, B. H., and Bailey, A. A.: The multi-institution North American Land Data Assimilation System (NLDAS): Utilizing multiple GCIP products and partners in a continental dis-

tributed hydrological modeling system, J. Geophys. Res., 109, D07S90, doi:10.1029/2003JD003823, 2004.

Potter, N. J. and Zhang, L.: Interannual variability of catchment water balance in Australia, J. Hydrol., 369, 120–129, doi:10.1016/j.jhydrol.2009.02.005, 2009.

Renner, M., Brust, K., Schwärzel, K., Volk, M., and Bernhofer, C.: Separating the effects of changes in land cover and climate: a hydro-meteorological analysis of the past 60 yr in Saxony, Germany, Hydrol. Earth Syst. Sci., 18, 389–405, doi:10.5194/hess-18-389-2014, 2014.

Shao, Q., Traylen, A., and Zhang, L.: Nonparametric method for estimating the effects of climatic and catchment characteristics on mean annual evapotranspiration, Water Resour. Res., 48, W03517, doi:10.1029/2010WR009610, 2012.

Troch, P. A., Carrillo, G., Sivapalan, M., Wagener, T., and Sawicz, K.: Climate–vegetation–soil interactions and long-term hydrologic partitioning: signatures of catchment co-evolution, Hydrol. Earth Syst. Sci., 17, 2209–2217, doi:10.5194/hess-17-2209-2013, 2013.

Van Genuchten, M. T.: A Closed-form Equation for Predicting the Hydraulic Conductivity of Unsaturated Soils, Soil Sci. Soc. Am. J., 44, 892–898, 1980.

Wang, D.: Evaluating interannual water storage changes at watersheds in Illinois based on long-term soil moisture and groundwater level data, Water Resour. Res., 48, W03502, doi:10.1029/2011WR010759, 2012.

Wang, T., Istanbulluoglu, E., Lenters, J., and Scott, D.: On the role of groundwater and soil texture in the regional water balance: An investigation of the Nebraska Sand Hills, USA, Water Resour. Res., 45, W10413, doi:10.1029/2009WR007733, 2009.

Williams, C. A., Reichstein, M., Buchmann, N., Baldocchi, D., Beer, C., Schwalm, C., Wohlfahrt, G., Hasler, N., Bernhofer, C., Foken, T., Papale, D., Schymanski, S., and Schaefer, K.: Climate and vegetation controls on the surface water balance: Synthesis of evapotranspiration measured across a global network of flux towers, Water Resour. Rese., 48, W06523, doi:10.1029/2011WR011586, 2012.

Xu, X., Liu, W., Scanlon, B. R., Zhang, L., and Pan, M.: Local and global factors controlling water-energy balances within the Budyko framework, Geophys. Res. Lett., 40, 6123–6129, doi:10.1002/2013GL058324, 2013.

Yang, D., Sun, F., Liu, Z., Cong, Z., Ni, G., and Lei, Z.: Analyzing spatial and temporal variability of annual water-energy balance in nonhumid regions of China using the Budyko hypothesis, Water Resour. Res., 43, W04426, doi:10.1029/2006WR005224, 2007.

Yang, D., Shao, W., Yeh, P. J. F., Yang, H., Kanae, S., and Oki, T.: Impact of vegetation coverage on regional water balance in the nonhumid regions of China, Water Resour. Res., 45, W00A14, doi:10.1029/2008WR006948, 2009.

Yokoo, Y., Sivapalan, M., and Oki, T.: Investigating the roles of climate seasonality and landscape characteristics on mean annual and monthly water balances, J. Hydrol., 357, 255–269, doi:10.1016/j.jhydrol.2008.05.010, 2008.

Zhang, L., Dawes, W. R., and Walker, G. R.: Response of mean annual evapotranspiration to vegetation changes at catchment scale, Water Resour. Res., 37, 701–708, doi:10.1029/2000WR900325, 2001.

Zhang, L., Hickel, K., Dawes, W. R., Chiew, F. H. S., Western, A. W., and Briggs, P. R.: A rational function approach for estimating mean annual evapotranspiration, Water Resour. Res., 40, W02502, doi:10.1029/2003WR002710, 2004.

Zhang, L., Potter, N., Hickel, K., Zhang, Y., and Shao, Q.: Water balance modeling over variable time scales based on the Budyko framework – Model development and testing, J. Hydrol., 360, 117–131, doi:10.1016/j.jhydrol.2008.07.021, 2008.